Experimental Studies of Liquid Crystal and Protein Interactions

A Major Qualifying Project

Submitted to the Faculty of the

WORCESTER POLYTECHNIC INSTITUTE

in partial fulfillment of the requirements for the

Degree of Bachelor of Science

By

Shaun A. Marshall

Date: April 29, 2013

Advisors:

Prof. Izabela Stroe

Prof. Germano Iannacchione

Department of Physics

Key Words: proteins, liquid crystals, experimental, DRS, DSC, polarizing light microscopy

This report represents the work of one or more WPI undergraduate students submitted to the faculty as evidence of completion of a degree requirement. WPI routinely publishes these reports on its website without editorial or peer review. For more information about the projects program at WPI, visit http://www.wpi.edu/Academics/Projects.

Abstract

The fundamental interactions between proteins and liquid crystals were studied using 4-Cyano-4'-pentylbiphenyl (5CB) and equine heart myoglobin in varying concentrations. Polarizing Light Microscopy was used to capture images of pure and mixed components, depicting a caging process of the 5CB by the myoglobin as it competes for interaction with water. Dielectric Relaxation Spectroscopy and Differential Scanning Calorimetry provided evidence of an inverse relationship between the hydrated-myoglobin/5CB ratio and charge carrier diffusion barrier energy and nematic-isotropic transition temperature respectively. A trend in the heat capacitance peak shift alludes to an additional process related to a possible optimum concentration, which correlates with the microscopy caging process analysis.

Acknowledgements

I would like to take a moment to express sincere gratitude to Parvathalu Kalakonda for his time and effort in attaining the differential scanning calorimetry data of the various specimen tested within Prof. Iannacchione's laboratory, John Arnold for acquiring the excellent images and videos with the polarizing microscope, and of course, my loving family and friends, whose care and support have helped me to complete this project to the best of my ability.

Contents

List of Tables

List of Figures

1 Introduction

The precursors to a number of diseases have been found to inhabit the blood, including Alzheimer's Disease, Parkinson's Disease, and Huntington's Disease [1, 2, 3]. Current viable diagnostic methods either require separating whole blood samples into plasma or serum, or are too costly or time-consuming [4, 5]. It is therefore our goal to construct a Lab-on-a-Chip method which can be used as a site of rapid point-of-care testing in the clinical setting to quickly assess the macromolecular composition of a minimal blood sample. This method will be able to sense and sort the various components of whole blood using liquid crystals (LC), whose use is motivated by recent advancements in their use as sensors and optical tools [6, 7, 8] (see Fig. 1.1 for visual reference). In order to develop such a method, the fundamental interactions between LC and biological specimen must be fully understood, which can be broken down into many individual studies. Our journey begins with the documentation of experimental responses of mixing LC and proteins.

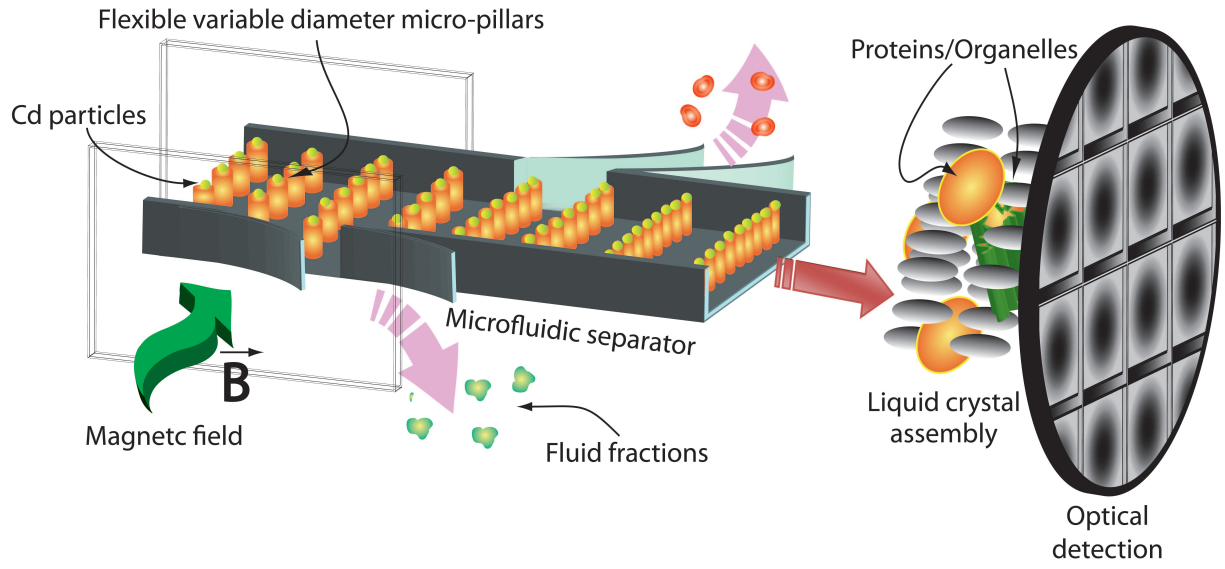

Figure 1.1: Cartoon representation of "Lab-on-a-Chip" Model.

1.1 Approach

To construct the Lab-on-a-Chip method, we must be capable of interpreting data which it collects. Studies have been performed on the mechanical [36] and optical [38] properties of reactions between LC and proteins, but there does not exist a universally accepted deterministic sensing/sorting mechanism of whole blood. Our sensing mechanism is compiled after the establishment of an experimental background, consisting of light polarizing microscopy, dielectric relaxation spectroscopy, and differential scanning calorimetry, of mixtures of LC and proteins. The microscopy allows us to obtain high resolution images of the birefringent material, whose light color, location, and intensity are all a function of the sample composition and structure. The DRS analysis provides information related to the collective dynamics of the LC-protein solutions, such as relaxation times and dielectric properties; important qualities such as dipole moments and activation energies are acquired. These activation energies can be confirmed with those received from the calorimetry techniques, which establish a referential basis of the varying heat capacities. Once we have information on the interactions of LC and proteins, studies can diverge into multiple paths, including comparisons with other types of proteins/macromolecules, computational analysis (such as Monte Carlo simulations), and initial designs of clinical use applications.

2 Literature Review

Theoretical and experimental models have been developed for the structure and properties of proteins and liquid crystals. Dielectric Relaxation Spectroscopy and Differential Scanning Calorimetry have been shown to be sensitive techniques for measuring properties of protein solutions, such as dielectric permittivity and specific heat capacity. Light Polarizing Microscopy allows for the observation of dual-refracting material in real time. While there is not extensive research in the basic interactions between proteins and LC, there have been initial uses of the two in experiments as integration into measurement equipment, and even a proof-of-concept for the LC biological material sensor.

2.1 Experimental techniques

In order to gain a fundamental understanding of the interactions between proteins and liquid crystals, we must first take into account the basic information attained from the different experiments applied. In our study, we utilize polarizing microscopy, dielectric relaxation spectroscopy, and differential scanning calorimetry.

2.1.1 Polarized Light Microscopy

Polarized light is defined as photons whose vibrations are limited to a single plane. This is accomplished in practice with the use of a removable slit. A polarizing microscope contains a couple of specialized accessories called a *polarizer* and an *analyzer*, which are made up of polarizing plastic [9]. The electric field vector of light is given by the equation

$$\vec{E} = E_{o,x} \cos(kz - \omega t)\hat{x}. \tag{2.1}$$

Equation 2.1 describes the upward motion of the light with maximum E-field amplitude $E_{o,x}$ and wavenumber $k = \frac{2\pi}{\lambda}$. When the E-fields are altered due to a polarization from two slits such as the setup of the polarizing microscope, the intensity follows the form

$$I = I_o \cos^2 \theta, \tag{2.2}$$

where θ in Eq. 2.2 is the angle between the polarizer and the analyzer, and I_o is the initial intensity of the light as set by the microscope. Our study demands complete polarization of light between the two components, meaning the angle is to be 90°; thus, only *birefringent* (or "doubly refractive") material specimen, which have different indices of refraction as a function of impinging light source location, are observed upon the otherwise dark background [9].

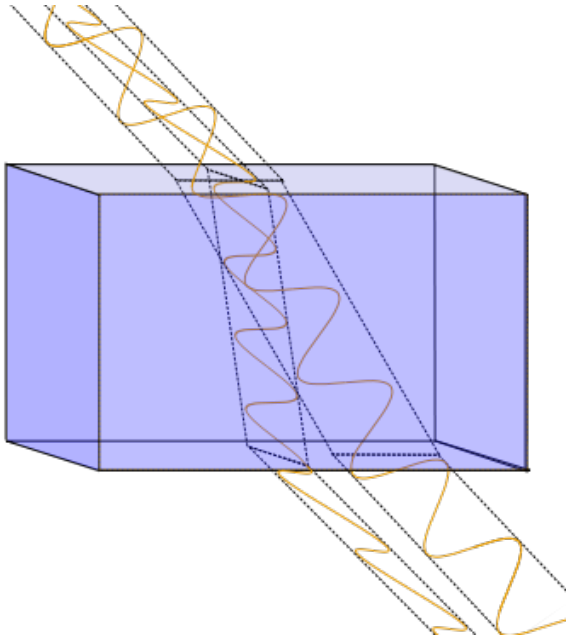

Figure 2.1: Cartoon of Birefringent Material [10].

Figure 2.1 depicts a visual of such a doubly refractive material, which means the index of refraction $\left(n = \frac{c}{v}\right)$ varies by location; this phenomena occurs in materials which are rigid or are composed of a repeated pattern structures.

2.1.2 Dielectric Relaxation Spectroscopy

The study of electromagnetic radiation absorption in materials, or *spectroscopy*, is related to the polarization of materials via an electric field. The classification of the polarization (Electron, Atomic, Orientational, Ionic, Electrode) is dependent on the frequency of the applied AC Voltage. There is a certain parameter of time-dependence to an alternating current induced potential, known as the *relaxation time*, which is the time required to achieve maximum polarization [12]. The observation of the change in the dielectric constant is of particular interest, and can be found from the impedence of an electric circuit $Z^*(\omega)$ (Eq. 2.3),

$$\epsilon^*(\omega) = \frac{1}{i\omega C_o Z^*(\omega)}, \tag{2.3}$$

with empty cell capacitance C_o, and ω, the variable AC current frequency [11]. The complex dielectric permittivity is usually fit with two functions as shown in Eq. 2.4:

$$\epsilon^*(\omega) = \epsilon'(\omega) + i\epsilon''(\omega) = -\left(\frac{\sigma_o}{\epsilon_o \omega}\right)^N + \epsilon^*_{HN}(\omega), \tag{2.4}$$

where

$$\epsilon^*_{HN}(\omega) = \epsilon_\infty + \frac{\epsilon_o - \epsilon_\infty}{(1 + (i\omega\tau)^\alpha)^\gamma}. \tag{2.5}$$

The initial term of the total dielectric response (Eq. 2.4) is the conductivity contribution due to electrode polarization, which plays an unfortunate parasitic role in the analysis of observed permittivity: σ_o is the DC conductivity and N is the exponential dependence term of frequency to conductivity [12]. $\epsilon^*_{HN}(\omega)$ (Eq. 2.5) is called the "Havriliak-Negami" function, named after the scientists who did extensive work in spectroscopic data analysis. ϵ_∞ is the permittivity at the high-frequency limit, ϵ_o is the well-known permittivity of free space, and τ is the relaxation time characteristic of the specific specimen being analyzed [11, 14]. The parameters α and γ are also empirically-found fitting terms. An additional Havriliak-Negami

function may be found to fit data which depicts more than one relaxation peak, as seen by Fig. 2.2.

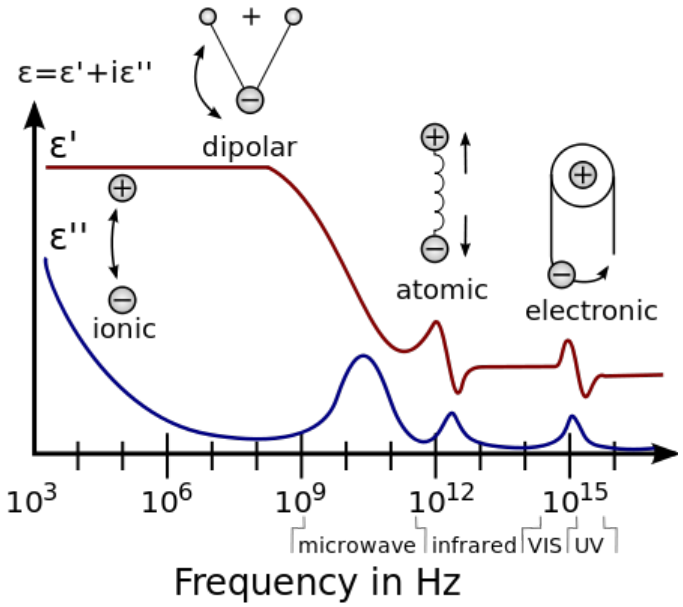

Figure 2.2: Typical graph of dielectric permittivity as a function of frequency, with corresponding physical interpretations of polarization [15].

The relaxation time is observed as large steps in the frequency (where $\tau \sim \frac{1}{f}$), which is apparent within Fig. 2.2 around 10^{12} Hz and 10^{15} Hz in the "real permittivity" (ϵ'), and as peaks in the "imaginary permittivity" (ϵ''); these frequency locations will vary depending on the material. There is a relationship between the location of the relaxation time frequencies (Eq. 2.6) and the temperature known as the Arrhenius Law (Eq. 2.6), which is used to determine the activation energy of the induced by the polarizing electric field:

$$\nu(T) = \frac{1}{\tau(T)} = \nu_\infty \exp\left(-\frac{E_A}{k_B T}\right). \tag{2.6}$$

The behavior shown in Eq. 2.6 tells us that the inverse of the relaxation time decays exponentially as a function of inverse temperature [16, 17, 13]; k_B is the Boltzmann Constant and ν_∞ is the high-temperature limit of relaxation frequency. Some materials may instead follow an altered relationship between temperature and relaxation time, given by the Vogel-

Fulcher-Tammann dependence:

$$\nu(T) = \nu_\infty \exp\left(-\frac{DT_o}{T - T_o}\right), \tag{2.7}$$

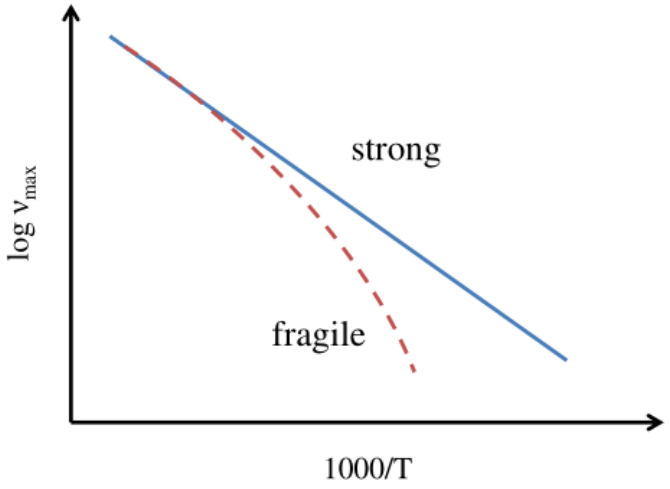

Figure 2.3: Comparative Arrhenius/VFT behavior [12].

where T_o in Eq. 2.7 is the mathematically limiting "Vogel-Fulcher Temperature", and D is a constant which describes the "fragility" of the relaxation peaks [16, 18]. These relationships are contrasted in Fig. 2.3.

We may also directly measure the conductivity as a function of AC frequency,

$$\sigma^*(\omega) = \sigma'(\omega) + i\sigma''(\omega) = i\omega\epsilon_o\epsilon^*(\omega). \tag{2.8}$$

A similar process can be found within the peaks in the measured conductivity, given by

$$\frac{1}{\tau_\gamma} = \frac{\sigma_o}{T} \exp\left(-\frac{E_\sigma}{k_B T}\right). \tag{2.9}$$

Aside from the experimentally determined prefactor σ_o in Eq. 2.9, the main feature is the application of this new energy, which for conductivity peak shifts is the barrier for charge carrier diffusion [19].

2.1.3 Differential Scanning Calorimetry

Calorimetry is the technique in which we may measure the flow of heat through a material. Differential Scanning Calorimetry obtains this heat flux measurement of a specimen relative to a reference, generally an empty container. Heat is applied to the two containers, and a multimeter is used to determine the potential (heat) difference between the containers. The ratio of the acquired potential difference to the applied increase in temperature (both of which as a function of time, experimentally) is known as the pressure-constant *heat capacity*, a material-specific property. The heat capacity for polymers (such as proteins) must be constantly increasing with respect to temperature; this is an *endothermic* process [22]. Dividing out the mass of the specimen used gives us the *specific heat capacity*,

$$\Delta c_p(T) = \frac{1}{m}\frac{\Delta Q/\Delta t}{\Delta T/\Delta t} = \frac{\Delta Q}{m\Delta T}; \tag{2.10}$$

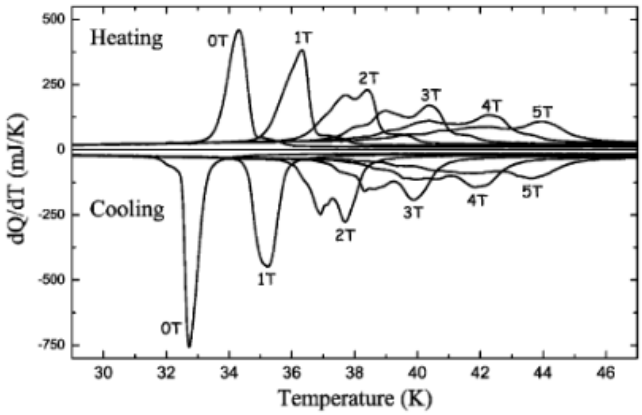

Figure 2.4: Calorimetric curves on heating and cooling for $ErCo_2$ under different applied fields.

these relationships are summarized in Eq. 2.10 [20]. Calorimetry is an ideal tool to locate the temperature of a phase transition of crystalline structures. Fig. 2.4 depicts the change in phase transition temperature due to the adjustment of an applied magnetic field [23]. The raw output from a calorimeter would certainly explicitly show the linear relationship between

heat capacity and absolute temperature, but to reduce noise and pinpoint phase transition location (where a thin, high-amplitude peak may be observed), the data is normalized by dividing the interpolated linear data.

2.2 Protein Structure and Dynamics

The amino acid, the subunit of a protein, is made up of three distinguishable groups extending from a central hydrocarbon ("CH"): the *amine* group ("$-NH_3$"), the *carboxlic* group ("$-COOH$"), and a *functional* group ("$-R$"). The functional group defines the classification of the amino acid, and can vary in structure from anything as simple as a hydrogen (as in Glycine) to Indole, an aeromatic, heterocyclic organic compound (as in Tryptophan). Amino acids which are bound together are called a polypeptide; a protein is a large polypeptide of specific amino acids. Our study involves myoglobin, which contains 153 amino acids, giving it a molecular weight of 17 kDa ($2.967 \cdot 10^{-20}$ grams) [21].

2.2.1 Physical Properties of Proteins

Proteins "activate", or readily undergo both intra-/intermolecular interactions, when they are hydrated (that is, treated with a solution with a nonzero concentration of water). These interactions within the solution can be experimentally measured when certain parameters are held constant, such as the concentration of the proteins to water, and temperature of the system (as it relates to Brownian dynamics). There are however, certain physical limitations to protein solutions, including hydration levels to maximize activity, and denaturing temperature, the threshold at which proteins biologically break down and "deactivate" [24]. For myoglobin, the optimum level of hydration is approximately 73 water molecules per protein, and the denaturing temperature is approximately 76°C [25].

2.2.2 Myoglobin Function

The role of the protein in the biological system is entirely dependent on the composition of the protein. Myoglobin in particular has been observed to facilitate the diffusion of oxygen in the muscle. It is routinely found to come about as a response mechanism to an uneven gradient of, or demand for oxygen, where it provides transport for oxygen molecules. This has been proven in both directions, with experiments in which the supply of oxygen in the heart decreases sharply when there is a direct blockage of oxymyoglobin, or when the gene encoded for the creation of these proteins are knocked-out (unexpressed) [26, 27], and in which oxygen flux increase in the presence of functional-form myoglobin [28].

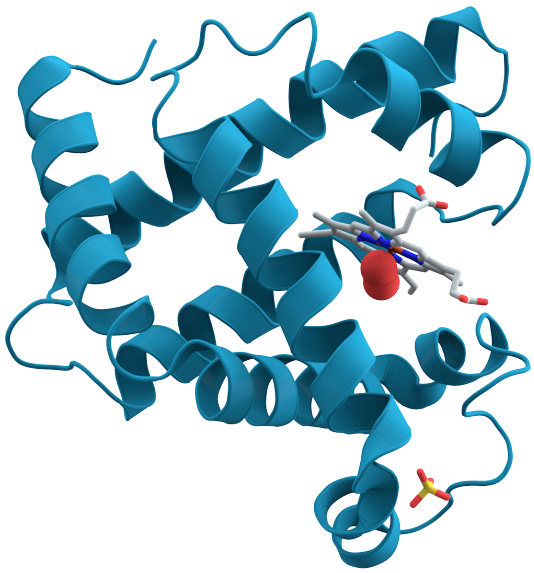

Figure 2.5: Cartoon Representation of Myoglobin[29].

We observe in Fig. 2.5 the particular geometries in the context of submergence in a hydration solution; we note that there is not only a limited surface area capable of interacting with bulk water (water not readily interacting with the protein) due to the size, but there exists a limited number of areas which are even available to interact with water due to the cross-folding pattern of the active protein.

2.3 Liquid Crystal Structure and Dynamics

The peculiar classification of matter known as liquid crystals (LC) are molecules which are very polarized, and contain additional matter-states than the common solid, liquid, and gas, due to their observed high molecular separation and kinetic energy. These additional states lie within the range of solid and liquid, each with varying degrees of structure and order, creating the "crystal"-like formations. The most common crystalline state is known as *nematic*, a helical structure which, specific to each LC, bend and block a quantifiable amount of light from being observed at some particular orientation. The common less-structured, greater distance state following the nematic phase is the *isotropic* phase [30].

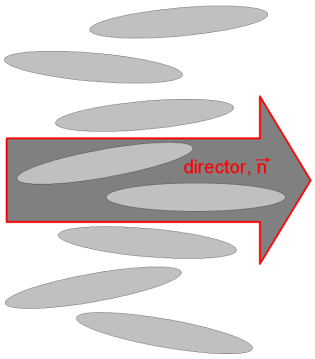

Figure 2.6: Cartoon Representation of the Nematic Director[31].

The orientation of a LC solution can be quantified; a popular approach (given as a conceptual descriptor) is the *Order Parameter*, given below

$$S = \langle P_2(\cos\theta) \rangle = \left\langle \frac{3\cos^2\theta - 1}{2} \right\rangle. \tag{2.11}$$

The angle θ within this molecular averaged *second order Legendre Polynomial* (Eq. 2.11) is that between the direction of the molecule and the *Nematic Director*, demonstrated in Fig. 2.6. The useful feature of this director is the extrema of its definition; $S = 0$ is inherent of a very random distribution of orientations, where $S = 1$ is a perfectly alligned sample of

molecules.

2.3.1 Physical Properties of Liquid Crystals

The rod-shaped liquid crystals like the ones shown in the cartoon of Fig. 2.6 are given the name *calamitic*, which is also the form of 5CB. LC which are found to exibit nematic phases generally follow the same structure: a terminal permenant diople of atomic components upon a single side, a flexible hydrocarbon chain on the other, and a binding of the formers with a fixed "rigid" core. Figure 2.7 demonstrates the previously mentioned geometries.

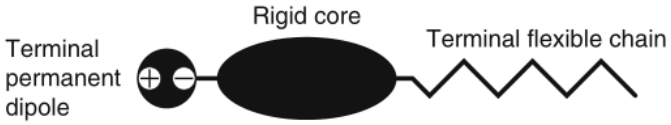

Figure 2.7: Cartoon Representation of Liquid Crystal.

A bulk property of nematic liquid crystals is its collective refractive index. The more structured the liquid crystals are, the more visible light is capable of passing through; visibility is directly proportional to the Order Paramter (Eq. 2.11). This is taken in conjunction with the transition temperature to the isotropic phase where the molecules become more disordered, to give us a useful function of the order in terms of temperature,

$$S = \left(1 - \frac{T}{T_{NI}}\right)^{b}. \tag{2.12}$$

The T_{NI} term in Eq. 2.12 is the crystal's known isotropic transition temperature, and b is an experimentally found parameter dependent on specimen and experimental setup [32].

2.3.2 5CB Studies

4-n-pentyl-4'-cyanobiphenyl (5CB) has been widely used in probing properties of liquid crystals. Classified as thermotropic (heat-gradient reactive), 5CB is often the choice for applications of optical displays, electromicroscopic components, and storage technologies [33].

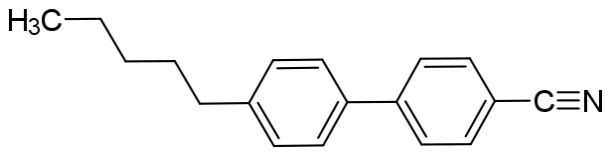

Figure 2.8: Cartoon Representation of 5CB [34].

We observe the predefined characteristics for a nematic liquid crystal as depicted in Fig. 2.7 within the representation of 5CB in Fig. 2.8. 5CB has a length of 20 $\mathring{A}$, a width of 5 $\mathring{A}$, a molecular weight of 249.4 g/mole, a crystalline-nematic phase transition at 22.5°C and a nematic-isotropic phase transition at approximately 35°C [35].

2.4 Current Research in Protein-LC Mixtures

The information in the mixing phenomena of proteins and liquid crystals is quite limited; primarily they are a tool of measurement rather than its specific properties, let alone the existance of effect of proteins *on* such properties.

2.4.1 Mechanical Phenomena

Optical studies involving the anchoring energies of liquid crystals have been performed. By attaching LC to the polarizer of a Light Polarizing Microscope, and calibrating the top of the analyzer (connected to the top of the liquid crystals) to be perpendicular to the polarizer, the LC torsion energies can be acquired from their interactions with biological media on the surface of the analyze [36]. Additional research has been performed in finding dissapation correlation between time-dependent adsorption of proteins and quartz crystal resonance frequencies [37].

2.4.2 Biosensors

5CB has been used as primitive qualitative sensor-imaging. A proof-of-concept model (Fig. 2.9) has been modeled recognizing the ability to differentiate liquid crystals contain-

ing a foreign specimen due to the change in overall order parameter, particularly biological specimen.

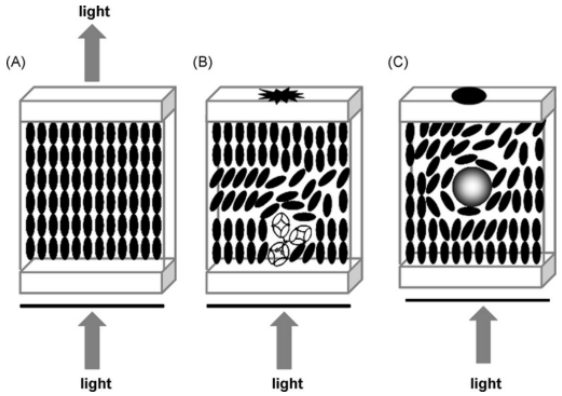

Figure 2.9: Cartoon Representation of LC Sensor Model [38].

Our end goal is to construct a model similar to this figure; this requires fundamental quantification of each component.

3 Methodology

Appendix A gives a detailed procedure of the preparation of each sample.

3.1 Materials

Samples were made using various combinations of deionized water [DI water] (no less than 18 $\Omega \cdot m$ resistivity), $\geq 90\%$ equine heart myoglobin (purchased from SIGMA Life Science), and 4-Cyano-4'-pentylbiphenyl liquid crystals [5CB] (purchased from Frinton Laboratories, Inc.). Sterile 2 mL vials were used for mixing and temporary storage.

3.2 Test Ratios

We prepared samples containing different mixing ratios of proteins and liquid crystals: pure 5CB, pure myoglobin and DI water, and a few particular mixtures which followed the rule given by the "mixture factor":

$$R = \frac{m_{Mb} + 2m_{H_2O}}{m_{5CB}}. \tag{3.1}$$

In Eq. 3.1, m_{Mb} is the mass of the myoglobin, m_{H_2O} is the mass of the DI water used, and m_{5CB} is the mass of 5CB used. For this experiment mixtures with an R value of 1 and 6 were used.

3.3 Polarizing Miscroscopy

Approximately 10 μL of each sample was plated on a sterile glass plate. The sample was spread evenly along the surface of the plate and observed using an AmScope polarizing microscope, with imagery and video captured by the prepackaged software. For samples containing any amount of 5CB, heat was gradually applied from the heating tray to a maximum of 50°C in order to attain a real-time observation of the transition between nematic

and isotropic phases.

3.4 Dielectric Relaxation Spectroscopy

The sample cell used in the Novocontrol Impedence Analyzer utilized about 1.5 mL of premade sample, which was carefully poured around the base, ensuring the lack of any bubbles along the surface. After placement of the cell in the analyzer, a broadband dielectric span of $6.69 \cdot 10^{-2}$ to $2.00 \cdot 10^{7}$ Hz was used to acquire responses of real/imaginary dielectric permittivity, as well as observed real/imaginary conductivity of the specimen. This measurement was repeated for all temperatures within the range of 50°C (40°C for pure 5CB) and -40°C in steps of 5°C. Liquid nitrogen was used for the cooling.

3.5 Calorimetry

Approximately 25 μL of each sample was dropped into the mini-cell and compressed shut. The TA Instruments Calorimeter environment received one empty mini-cell as a control, and the sample cell. The cells were heated in steps of 0.01°C to maximum temperature of 50°C, before cooling with liquid nitrogen to 20°C.

4 Results and Discussion

Plots were created using Gnuplot. Additional images can be found in Appendix B. Microscopy videos available upon request.

4.1 Polarized Microscopy

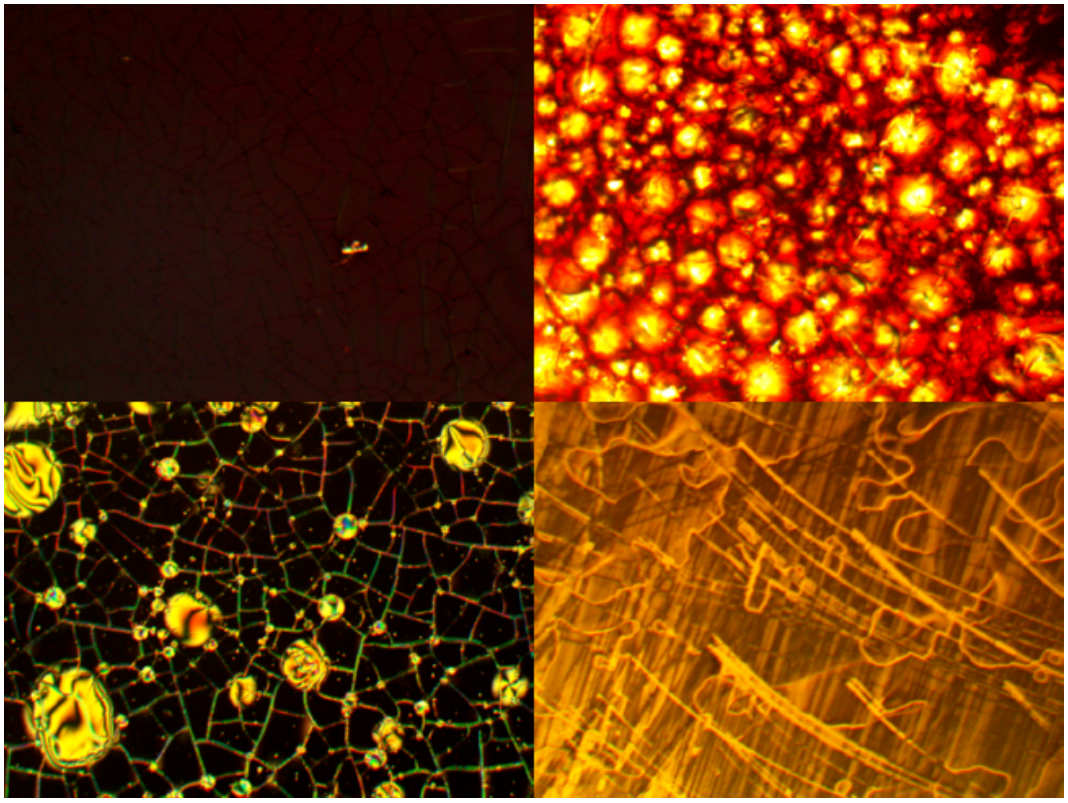

Figure 4.1: Polarized light microscopy images of a) [top-left] Pure myoglobin at 100x, b) [top-right] R=6 mixture at 200x, c) [bottom-left] R=1 mixture at 200x, d) [bottom-right] pure 5CB at 100x.

Figure 4.1 show images for different samples of mixures R=0,1,6,∞. It was found that the pure myoglobin depicted two distinct phenomena: a deep red color of various shades depending on the location, and a structural pattern of randomly oriented rods. A separate image of myoglobin (Fig. B.8) confirmed the the rods to be closely positioned individiuals and not borders of aggregations by the dispersement of the rods along the edge of the sample

where it has a more freedom to move in the DI water medium. The bright spot right of center in the pure myoglobin image was determined to be a biorefringing contamination.

A gradient of yellow and gold was characteristic of the liquid crystal samples. The phase-transition video acquired depicted a completely or major blackout of the specimen as the phase of the crystals changed to the more liquid isotropic state, breaking the polarized structures and eclipsing the underlying light source. The large curvatures found in the pure liquid crystal image were found to be arbitrary peaks in the nematic structure, proven by the melting and recooling of the 5CB, and a complete reposition of the curvatures. The long streaks through the center of this image was an over-scraping of the glass plate during the cleaning process.

The mixture sample images shows the characteristics of both myoglobin and 5CB, as well as some additional information. Where there is a presence of relatively more myoglobin (R=6), the deep red of the myoglobin is much more prevalent. In a similar manner, the addition of more 5CB compared to this (R=1) shows a greater radiance of the yellow-gold color. Both mixture images show the previously described rod-like structures of the myoglobin. Uniquely, these images also contain sphere-like structures, outlined in red and filled in with yellow-gold; this is a much greater presence of these spheres in the R=6 image.

The heating of the solutions containing liquid crystals were found to have a varied phase-transition temperature in the range of 40 and 50°C.

4.2 Dielectric Relaxation Spectroscopy

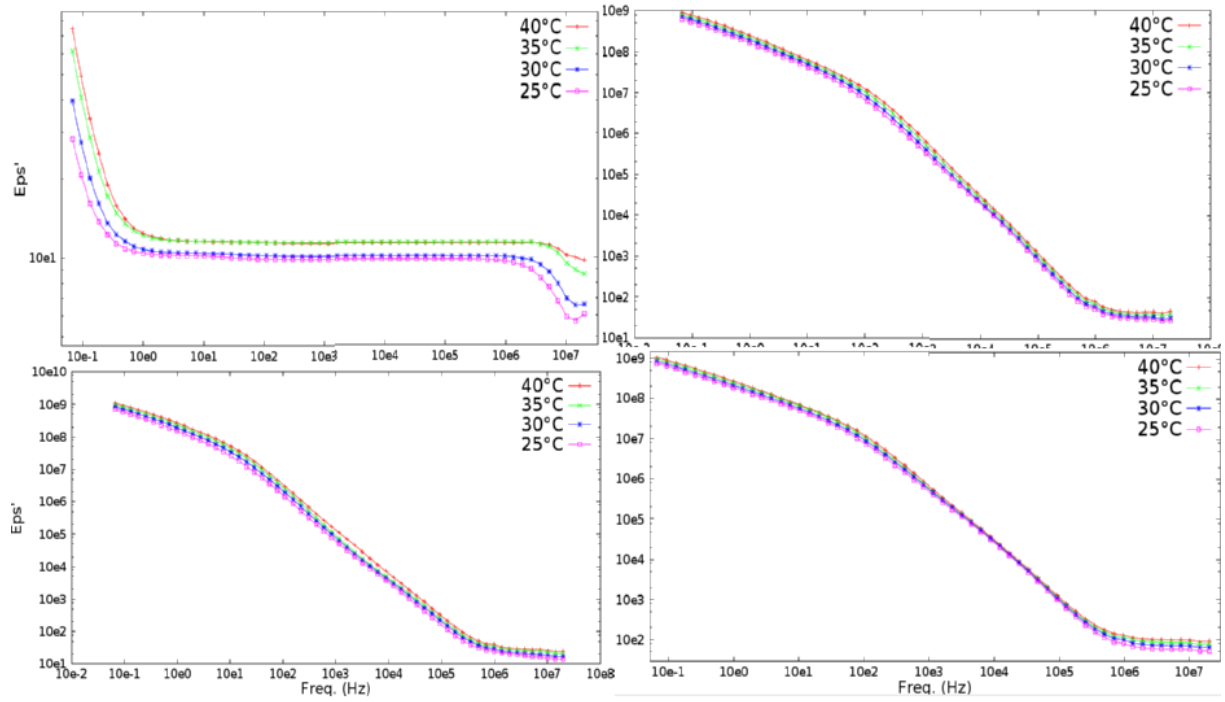

Figure 4.2: Real-part of Dielectric Permittivity at Varying Temperatures of a) Pure 5CB [top-left], b) Mixer R=6 [top-right], c) Mixer R=1 [bottom-left], d) Pure Myoglobin [bottom-right]

There are very small changes in the temperature-dependent shift of the real part of the dielectric permittivity, shown in Fig. 4.2. The response from the pure 5CB (R=0) is virtually constant over a large span of the frequency at such high temperatures; subzero temperatures did, however, show an explicitly shifting response peak (omitted). The initial increase of myoglobin concentration (R=1) depicts a massive jump in real permittivity over the spectrum, particularly low frequencies; the reader may observe this from the large scale change in all results of myoglobin-containing samples. As the concentration of myoglobin increases (R=6 to R=∞), the responses continues to marginally increase, with pure myoglobin data in extreme proximity to the R=6 mixer, only very slightly higher. Additionally, the increase in temperature also increases the magnitude of overall responses for all samples.

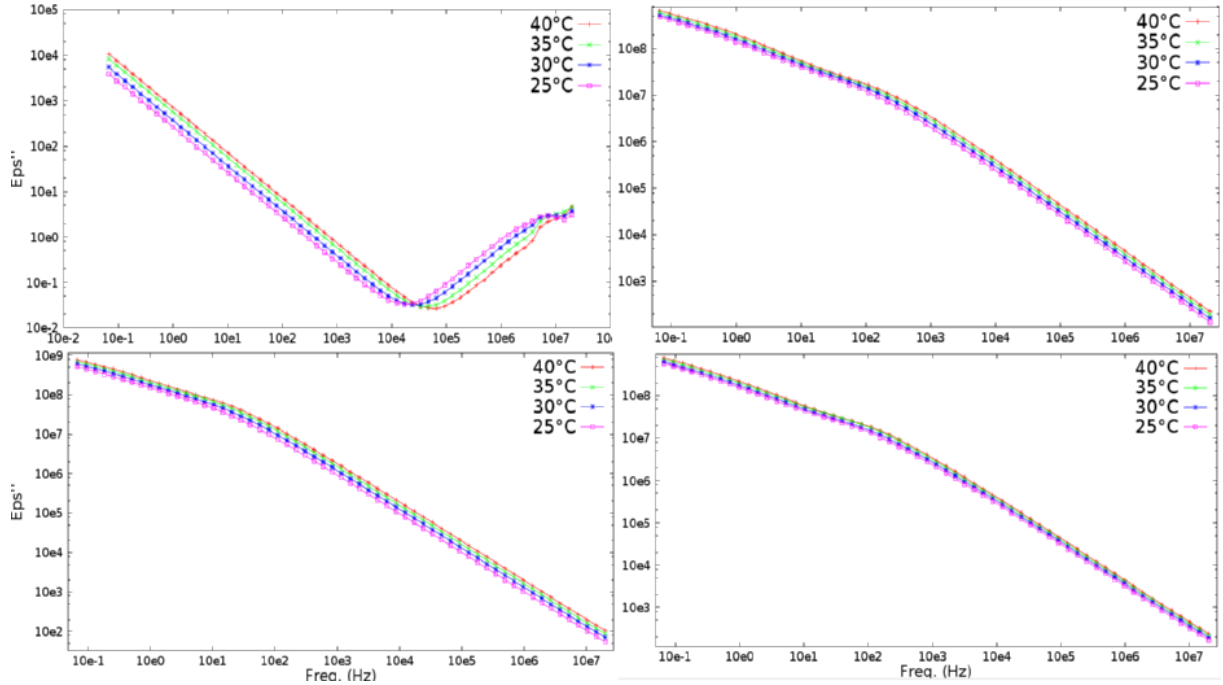

Figure 4.3: Imaginary-part of Dielectric Permittivity at Varying Temperatures of a) Pure 5CB [top-left], b) Mixer R=6 [top-right], c) Mixer R=1 [bottom-left], d) Pure Myoglobin [bottom-right]

The general trend of the imaginary part of the dielectric permittivity (Fig. 4.3) is an increase in magnitude proportionally with temperature. Again, the addition of myoglobin increases the magnitude of the response across the entire spectrum. Figure 2.2 informs us that the existance of relaxations are depicted by peaks within the imaginary permittivity, which is only prominent in the pure 5CB; all other samples are void of explicit peaks. The peaks found in the 5CB sample at around 10^7 Hz line up with the large upward step in the real permittivity response of 5CB (Fig. 4.2), suggesting there is indeed an activation energy associated with 5CB observable at high temperatures.

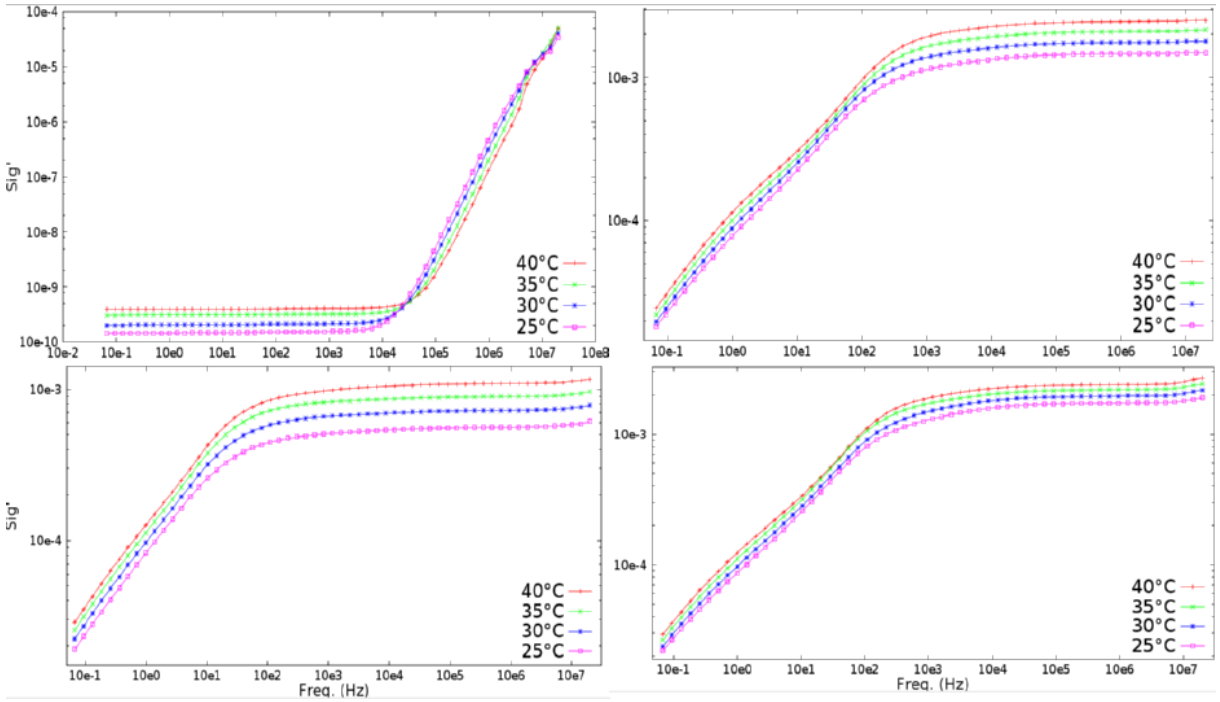

Figure 4.4: Real-part of Conductivity at Varying Temperatures of a) Pure 5CB [top-left], b) Mixer R=6 [top-right], c) Mixer R=1 [bottom-left], d) Pure Myoglobin [bottom-right]

Simultaneously, information on the conductivity of each sample was acquired, and can be found in Fiq. 4.4. We observe, for each sample, a peak frequency at which the real conductivity gradually begins (in the case of pure liquid crystal) or ends (otherwise) an exponential portion. This "shoulder" is measured as a function of the varying temperature, and is used to construct an Arrhenius plot (Appendix C). We observe an increase in magnitude of conductivity across the spectrum for all myoglobin-containing samples, but an inverse effect on the high-frequency side of the peak frequency in pure 5CB.

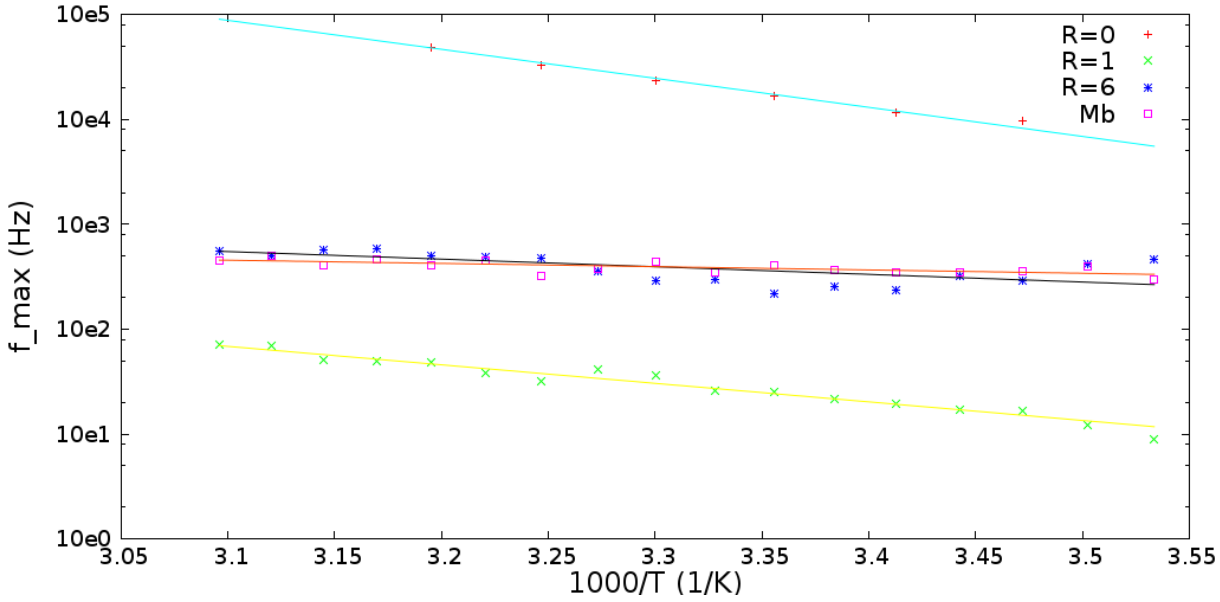

Figure 4.5: Arrhenius Plots and Curve Fits of Pure 5CB, Pure Myoglobin, and Mixers R=1,6

The Arrhenius-like relationship between conductivity peak frequencies and corresponding sample temperature are shown in Fig. 4.5, along with the linear behavior derived from the conductivity Arrhenius equation (Eq. 2.9):

$$log\left(\frac{1}{\tau_\gamma}\right) = log(\sigma_o) - \frac{E_\sigma}{k_B}\left(\frac{1}{T}\right) - log\left(\frac{1}{T}\right). \tag{4.1}$$

The corresponding parameters for each fit function are found in table 4.1:

Table 4.1: Arrhenius Fit Curve Parameters

Sample	Amplitude (σ_o) [Hz]	Energy (E_σ) [k_B]
5CB ($R = 0$)	$2.71 \cdot 10^{13}$	6.67
1:1 Ratio ($R = 1$)	$1.68 \cdot 10^{7}$	4.37
6:1 Ratio ($R = 6$)	$8.04 \cdot 10^{4}$	1.97
Mb ($R = \infty$)	$3.45 \cdot 10^{3}$	1.02

It is essential to note that both the amplitude and corresponding charge diffusion barrier

energy shift inverse-proportionately as a function of increasing concentration of myoglobin.

4.3 Calorimetry

Heat capacitance as a function of a range of temperatures is linear for materials with no phase change within that range, as we observe from Fig. 4.6 below.

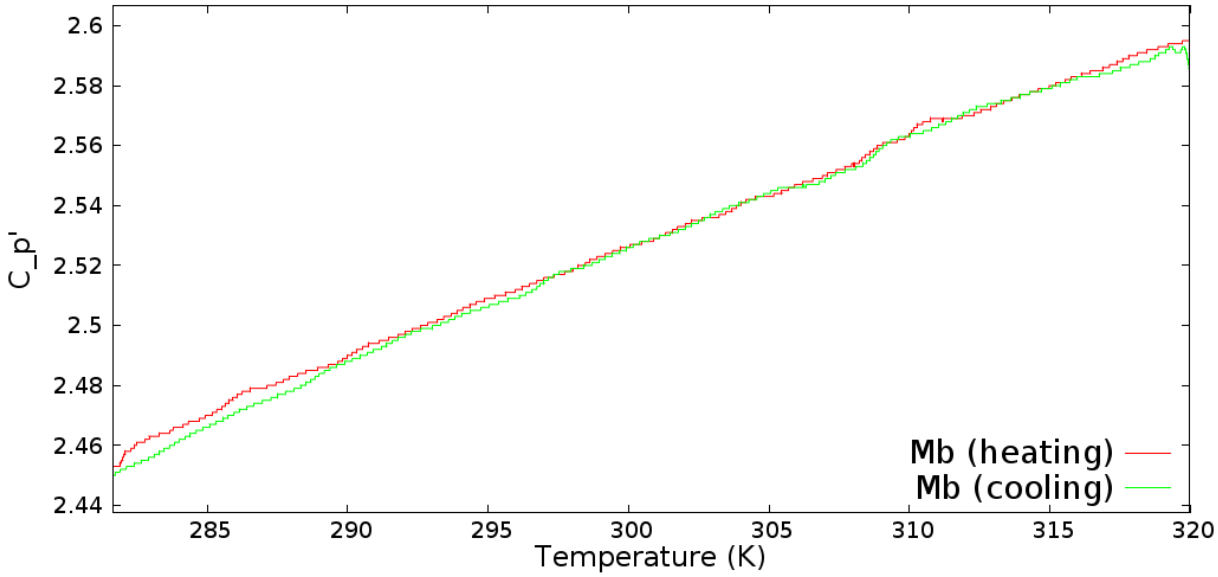

Figure 4.6: Real-part of Heat Capacitance for Myoglobin

With the addition of the liquid crystals, there is an apparent narrow peak of heat capacitance which occurs due the phase transition between the nematic (left side of peak) and isotropic (right side of peak) states (Fig. 4.7).

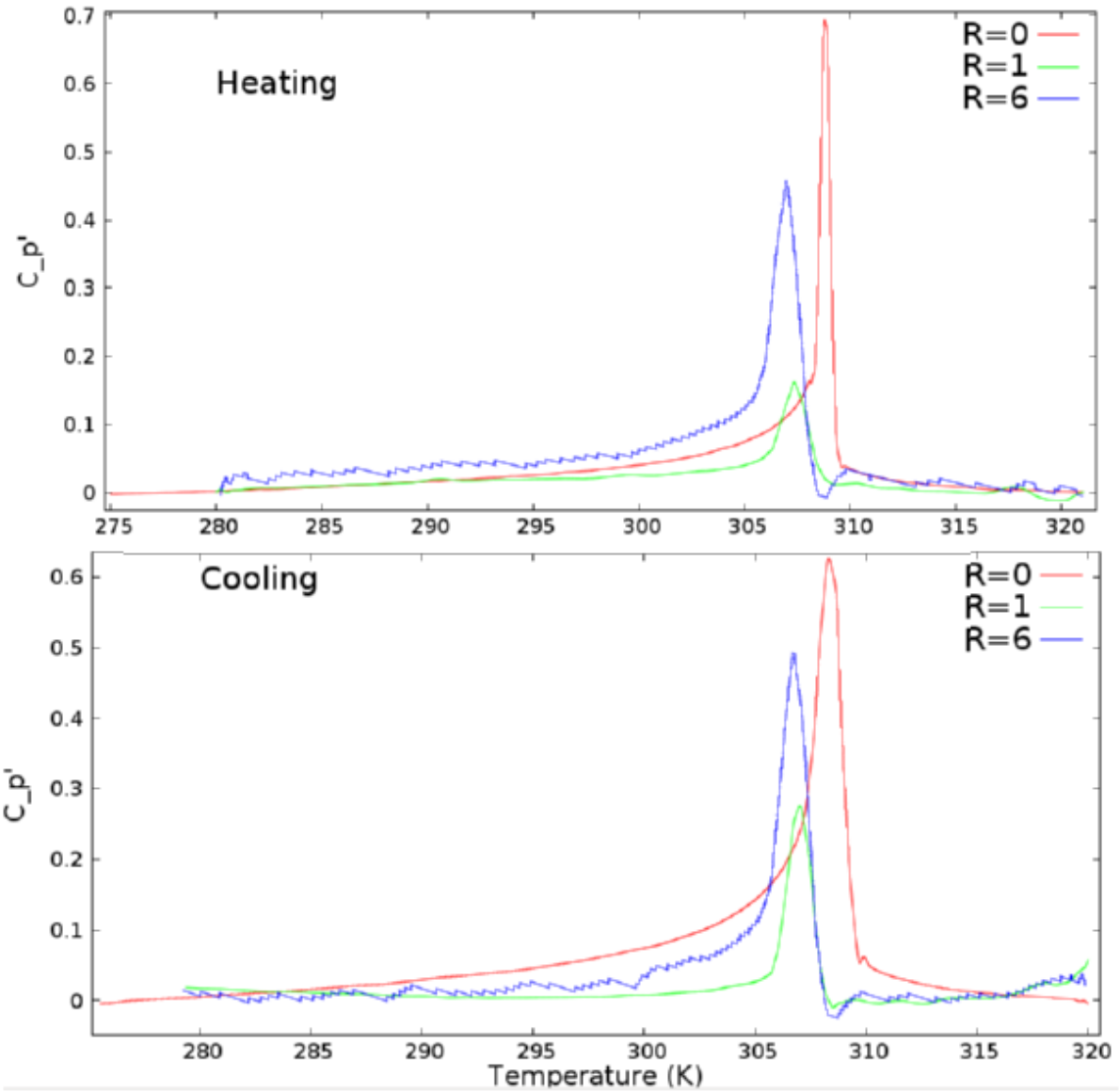

Figure 4.7: Real-part of Heat Capacitance for Samples Containing 5CB

We observe that the increase of the concentration of myoglobin (increase in R) proportionally decreases the temperature of the phase transition of the liquid crystals (Fig. 4.7). However, we observe an interesting progression of the amplitude of the heat capacity peak, decreasing from pure 5CB, to the 6:1 concentration (more myoglobin), to the 1:1 concentration (less myoglobin).

4.4 Discussion

The initial goal of the project was to determine the fundamental properties of the interactions of proteins and liquid crystals; this lead us into the quantitative analysis of whether the process could be described as either a linear combination of properties, or if a separate process arose. Upon inspection of the data, our conclusion is that both occur, to a degree. The images obtained from the light polarizing microscope clearly depicted red-tinted structured cracks as indication of the presence of myoglobin, and a smooth, glossy, yellow-gold surface as presence of 5CB. When mixed, there was an interesting visual effect, in which finite spherical "globs" of red and yellow formed. It certainly seems as though the proteins are mechanically interacting with the 5CB; whether it is chemically leaves room for further analysis.

These orbs also seem to be structured in such a way that the proteins are actually on the outer surface. It is already known that the myoglobin interacts with water to become hydrated and active. It was also empirically found that the liquid crystals did not mix well at all with the water. It is therefore plausible that the presence of liquid crystals and deionized water creates a competition for the protein, in which each polypeptide attempts to bond to either, depending on availability and molecular proximity; the result of this much be the orbs created (the more finite amounts liquid crystals themselves would initialize an orb via a seed), with the hydrophylic proteins on the surface, and hydrophobic liquid crystals in the core.

The dielectric permittivity certainly had a peculiar set of comparative responses. The order of magnitude of the response increased up to eight-fold, particularly around the low-frequency spectrum when half of the sample by weight became myoglobin compared to pure liquid crystals. This is massive compared to the marginal increases of myoglobin concentration, even up to the pure myoglobin, each step higher than the previous. The evidence provided here is inconclusive to the behavior of the mixture, as it is not currently understood what occurs for mixture factors of $R<1$; if the lower factors do not depict proportionatly lower responses, it may lead to the stronger argument of the existance of mixing phenomena.

We further analyzed the overall conductivity of the sample and observe a more exaggerated peak frequency shifting as a function of temperature. The shift in locations of these peak frequencies (shown in the Arrhenius plot in Fig. 4.5), are observed to be *indirectly proportional* to the concentration of myoglobin within the sample; that is to say, **the increase of myoglobin causes a decrease in the conductive charge carrier diffusion barrier energy of 5CB**.

Calorimetric analysis of the samples marked the location of the isotropic-nematic phase transition with a large peak in the heat capacitance at certain temperatures, among otherwise normalized data. While there is currently no explanation for the scattered heat capacitance peak amplitudes as a function of myoglobin addition, it was nonetheless observed that **the increase of myoglobin causes a decrease in the nematic-isotropic phase transition temperature of 5CB**. This correlates with the DRS data, as a lower temperature is needed to acquire a molecular barrier energy, which decreases with myoglobin addition.

It is possible that the scattered trend of heat capacitance amplitude and permittivity/conductivity amplitude shifts are related to the competition for the protein between the liquid crystals and the deionized water, as shown in the polarized microscopy images. The outlying data from both DRS and DRS may allude to an *optimum* ratio of liquid crystals and proteins within a water solution, in which the dielectric and calorimetric response are, in fact, constantly proportionally decreasing, with the exception of an outlying range of concentrations, from which a peak may be found (similar to the peaks found in the DSC graphs [Fig. 4.7]). Indeed, a large range of sample concentrations, including those of mixing ratios R<1 would be required to investigate this further.

5 Summary and Future Work

The experiments performed used 5CB and myoglobin as survey instruments in our search for understanding the fundamental interactions between proteins and liquid crystals. Light Polarizing Microscopy (LPM) was used to obatin images, and Dielectric Relaxation Spectroscopy (DRS) (coupled with an Arrhenius-relationship analysis) along with Differential Scanning Calorimetry (DSC) were used to acquire quantitative information on the LC-Protein systems.

5.1 Summary

Different concentration ratios (by weight) of 5CB and hydrated myoglobin were analyzed, following the form of Eq. 3.1 for R=0,1,6 and ∞. LPM was used to acquire a qualitative comparison of these samples, including videos of the phase transitions from samples containing LC; it was found that myoglobin showed up as a deep red spattering of lines, 5CB as a smooth yellow-gold. Combinations depicted both red and gold colors along with the phenomena of orbs. DRS was used to collect information on the permittivity and conductivity of the samples, the latter of which was further analyzed to project the corresponding charge carrier diffusion energies from the shift in peak frequencies. Both the relaxation rate (Arrhenius Law amplitude) and barrier energies were found to be inversely proportional to the increasing ratio of myoglobin to 5CB. DSC was used to locate the temperatures of the phase transition of 5CB given different added concentrations of myoglobin through changes in heat capacitance. These temperatures also decreased proportionally with myoglobin, but the heat capacitance amplitude followed an interesting shift, in which what seems to be an outlier was obtained around the value of R=1.

5.2 Future Work

As stated above, this work represents a survey, an initial attempt at the understanding of how liquid crystals and proteins interact. It was found through both DRS and DSC that an inverse-proportionality exists between the ratio of proteins to liquid crystals; in order to understand this relationship more fully, a larger array of concentrations must be assessed. The current speculation is that there may lie an optimum ratio, which physically correlates to the competition between water and LC for proteins, and which also may correlate to the outlying heat capacitance peak; to prove or disprove this idea, concentrations, particularly in the range of R<1 must be assessed, to determine whether this optimum exists, or if any nonzero addition of proteins causes a dramatic change in data. Analysis of concentrations of R>6 will allow for the determination of the existance of proportionality beyond this initial range of possible optimization.

It is possible that the phenomena we observe is also only inherent to the particular specimen used. With different molecular geometries, we may find that the these same procedures give either more or less predictable results if other proteins, Aβ 1-42 for instance, was used in place of myoglobin, or if 8CB was used in place of 5CB as the liquid crystal. A conclusion was reached just on the images that the proteins cage the liquid crystals in the process of competition; this is a geometry-dependent conclusion; it is possible that different shapes, if any, are found with different materials.

Appendices

A Sample Preparation

Cleaning of all tools and the sample cell involved ultra-frequency fluid shock within mediums of acetone and isopropanol, and rinsed with deionized water. Metal tools and cell components received heat during the shock treatment and were dried in a small oven, with tilt applied to the heat gradient so as to avoid heat spots on the surface.

Every prepared sample utilized a 2 mL sterile plastic vial which was zeroed on a scale for ease of mass-measurements. Mixtures involving myoglobin were treated with great care during transportation, which utilized a small metal spatula, so as to not lose any more than negligible amount of the powdery material. The myoglobin was added before the deionized water in order to avoid creating a hydrated mess on the spatula, which was constantly dug into the myoglobin jar. After the DI water was added to the test tube, it was shaken vigorously in order to evenly distrbute the hydration and attempt to create as homogenous mixture as possible. The pure myoglobin sample required more volume for proper mixing, so a sterile 10 mL beaker was used. The shaking was then simple replaced by cautious stirring. After mixing, it was transferred into a 2 mL vial.

5CB was added at the end of any mixture preparation in the 2 mL vial. It was noted that the 5CB didn't particularly mix well with water on the macroscopic scale, so vigorous shaking was applied, in order to simulate a homogenous mixture.

1.5 mL of the sample was transferred to the sample cell of the impedence analyzer, which was immediately placed in the containment center of the analyzer, and the sample was run.

B Microscopy Images

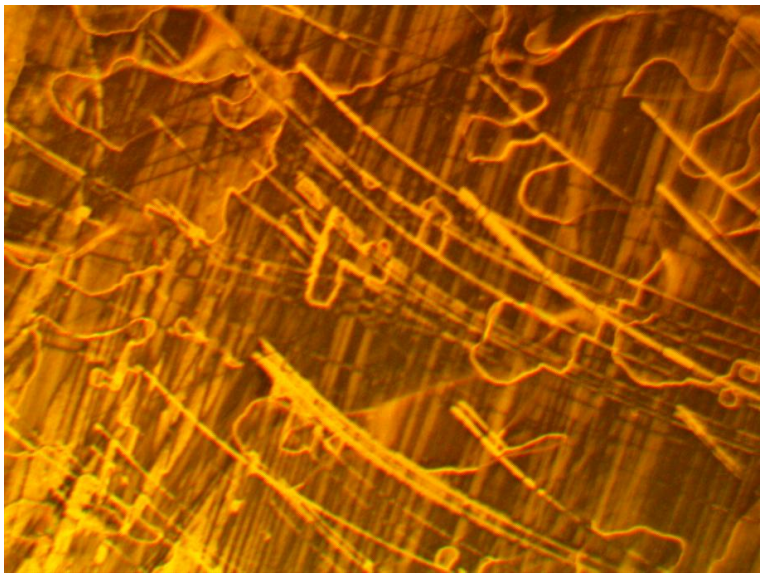

Figure B.1: Polarized Microscopy of 5CB at 100x zoom (as used in text).

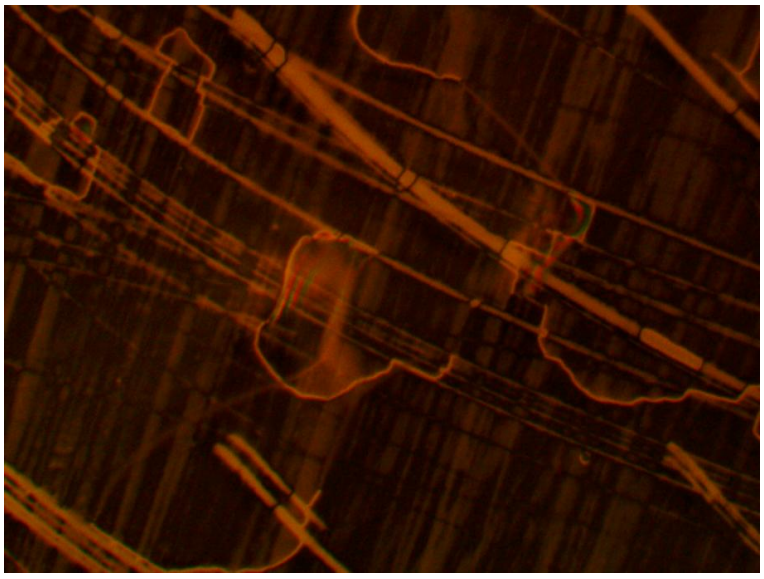

Figure B.2: Polarized Microscopy of 5CB at 200x zoom.

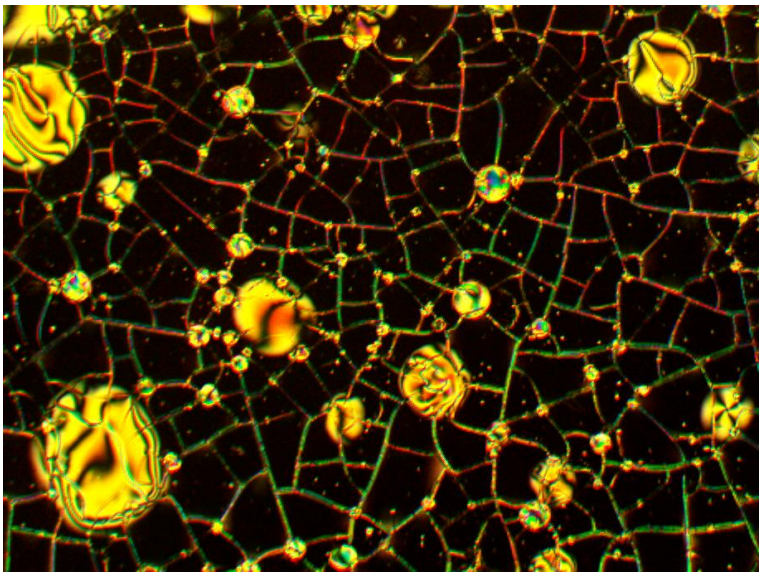

Figure B.3: Polarized Microscopy of R=1 concentration 200x zoom (as used in text).

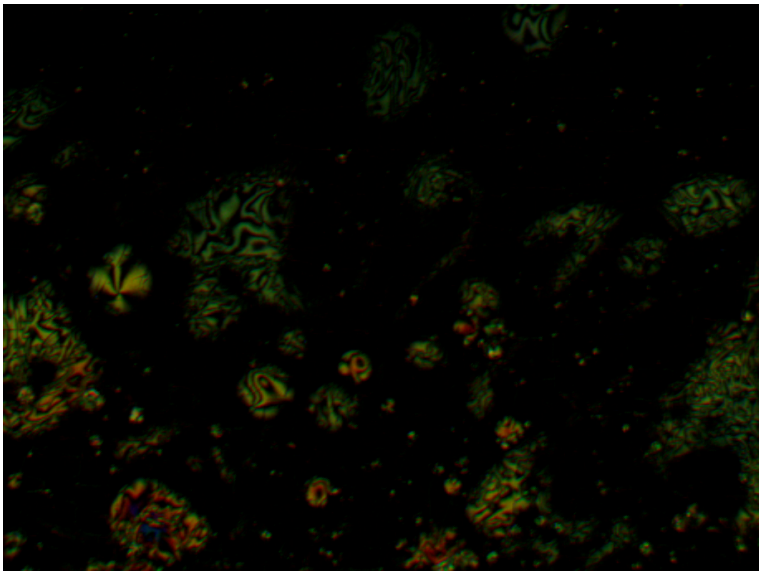

Figure B.4: Polarized Microscopy of R=1 concentration at 100x zoom in isotropic phase.

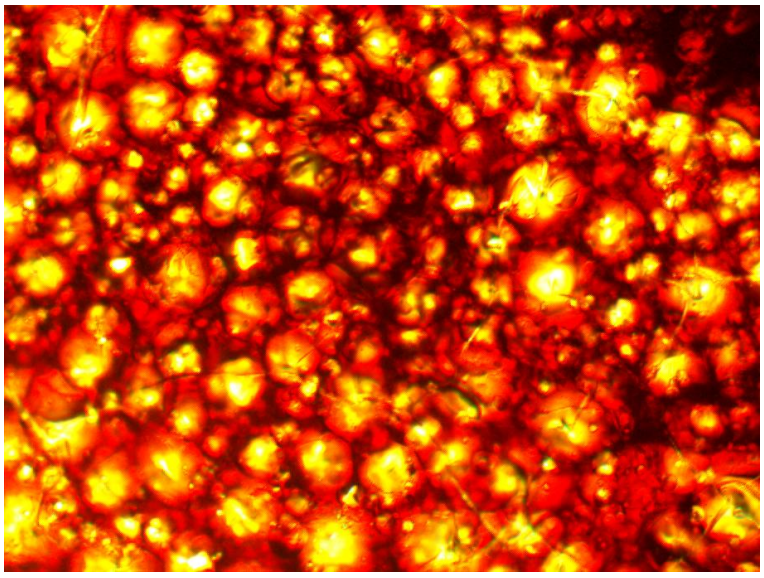

Figure B.5: Polarized Microscopy of R=6 concentration 100x zoom (as used in text).

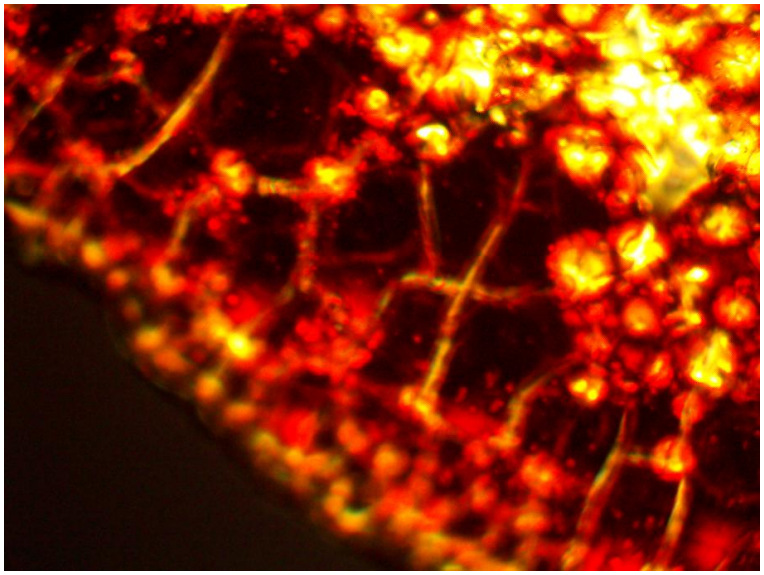

Figure B.6: Polarized Microscopy of R=6 at 100x zoom along edge of sample.

Figure B.7: Polarized Microscopy of myoglobin at 100x zoom (as used in text).

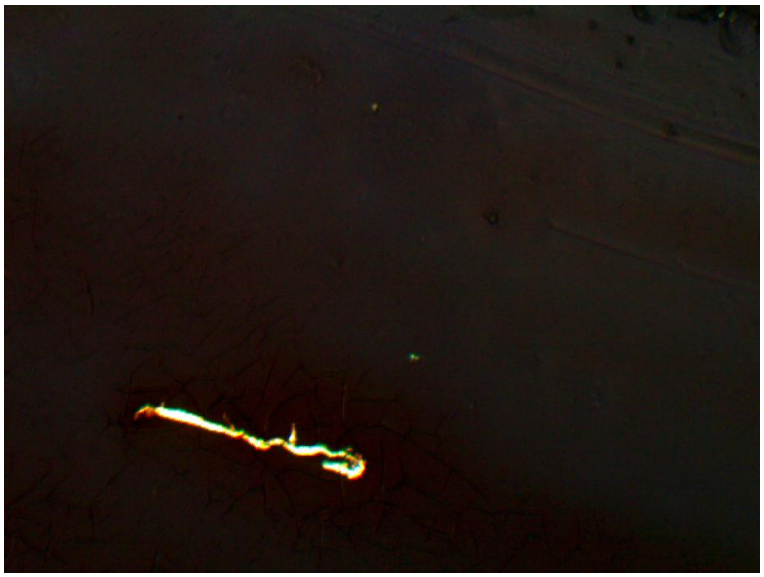

Figure B.8: Polarized Microscopy of myoglobin at 100x zoom along edge of sample.

C Arrhenius Plot Construction Approximations

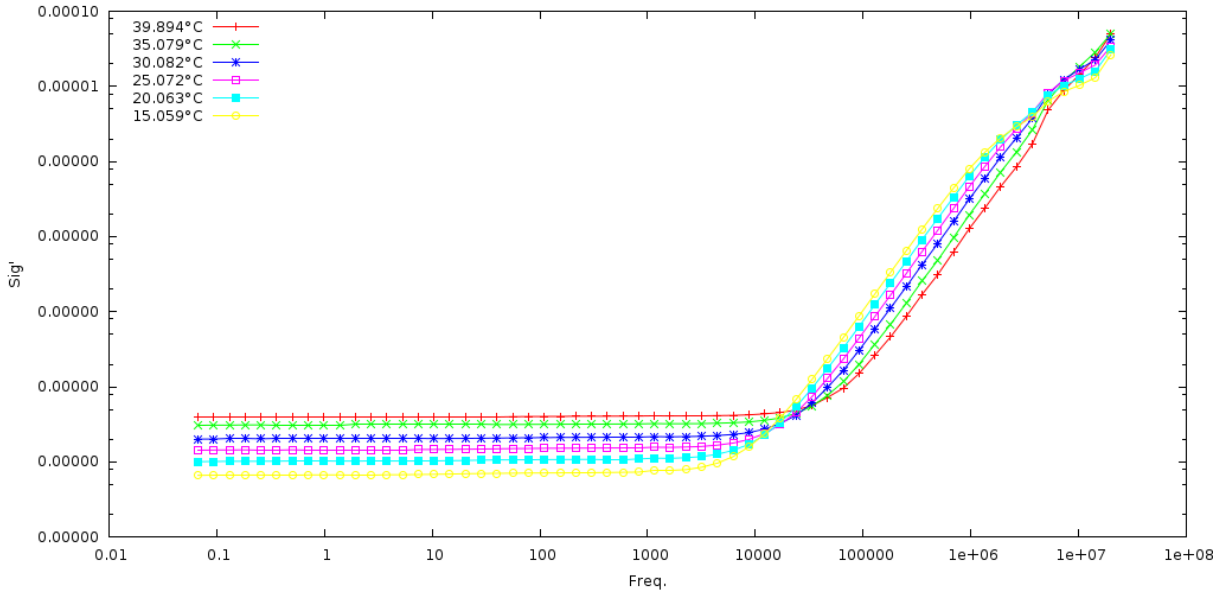

Figure C.1: Real Conductivity of 5CB

Table C.1: Arrhenius Data of Pure 5CB

Temperature (°C)	1000/T (K^{-1})	Peak Freqs (Hz)
40	3.195	47863
35	3.247	32609
30	3.300	23675
25	3.356	16632
20	3.413	11710
15	3.472	9655

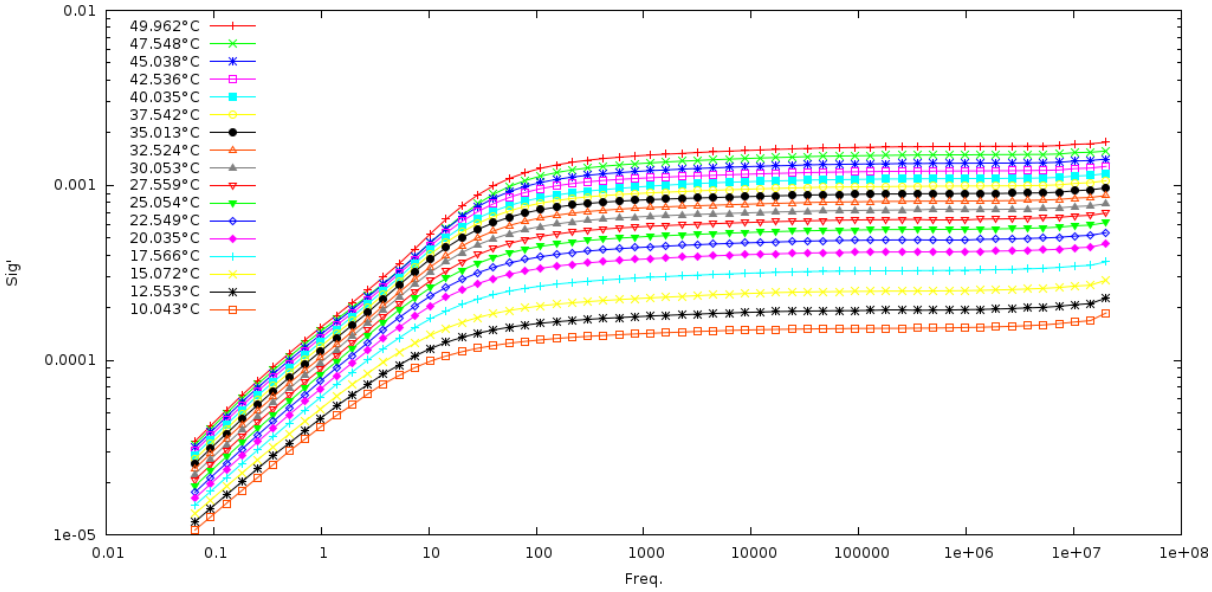

Figure C.2: Real Conductivity of Mixer R=1

Table C.2: Arrhenius Data of Mixer R=1

Temperature (°C)	1000/T (K^{-1})	Peak Freqs (Hz)
50	3.096	70.535
47.5	3.120	68.766
45	3.145	50.707
42.5	3.170	49.436
40	3.195	48.197
37.5	3.221	38.352
35	3.247	32.108
32.5	3.273	41.388
30	3.300	36.454
27.5	3.328	25.550
25	3.358	24.909
22.5	3.384	21.390
20	3.413	19.325
17.5	3.442	17.021
15	3.472	16.594
12.5	3.503	12.236
10	3.534	9.0229

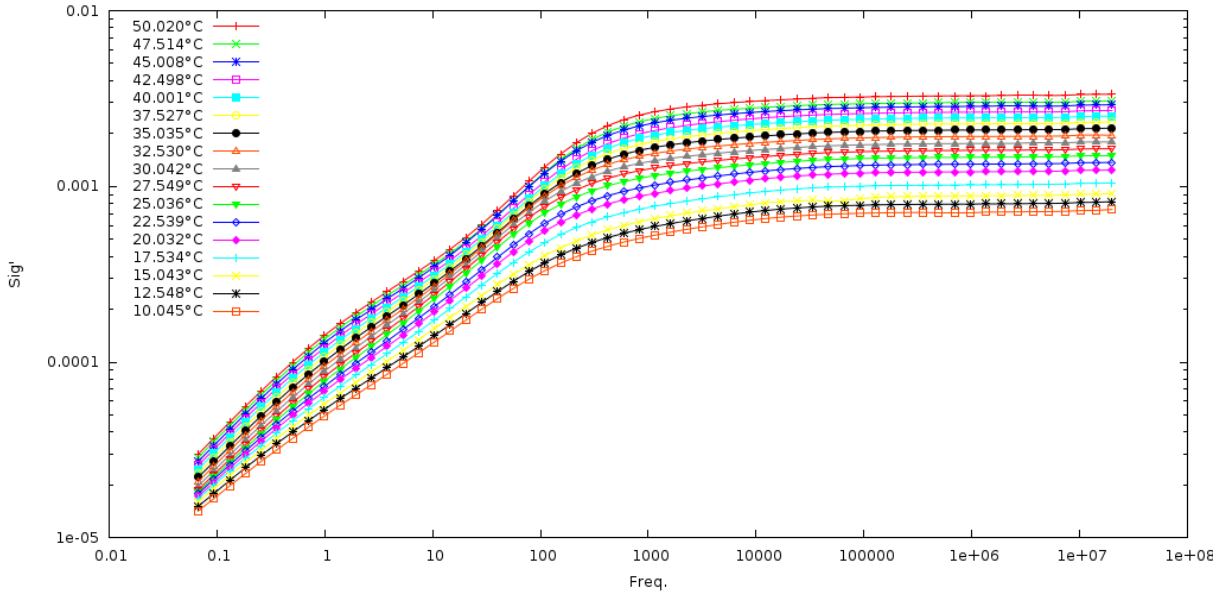

Figure C.3: Real Conductivity of Mixer R=6

Table C.3: Arrhenius Data of Mixer R=6

Temperature (°C)	1000/T (K^{-1})	Peak Freqs (Hz)
50	3.096	558.042
47.5	3.120	498.143
45	3.145	565.563
42.5	3.170	580.104
40	3.195	498.143
37.5	3.221	485.656
35	3.247	473.482
32.5	3.273	358.116
30	3.300	292.295
27.5	3.328	299.810
25	3.356	215.535
22.5	3.384	257.451
20	3.413	232.591
17.5	3.442	323.536
15	3.472	292.295
12.5	3.503	417.039
10	3.534	461.613

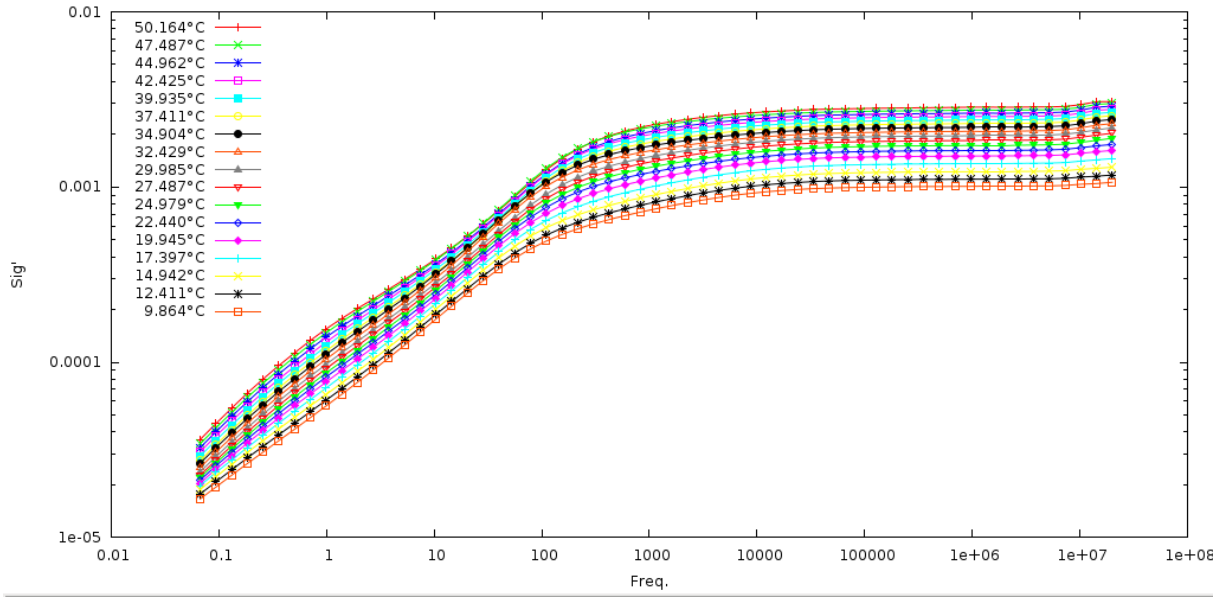

Figure C.4: Real Conductivity of Pure Myoglobin

Table C.4: Arrhenius Data of Pure Myoglobin

Temperature (°C)	1000/T (K^{-1})	Peak Freqs (Hz)
50	3.096	450.833
47.5	3.120	498.907
45	3.145	407.391
42.5	3.170	462.399
40	3.195	407.391
37.5	3.221	450.833
35	3.247	324.340
32.5	3.273	377.597
30	3.300	439.556
27.5	3.328	349.949
25	3.356	407.391
22.5	3.384	368.135
20	3.413	349.949
17.5	3.442	349.949
15	3.472	358.926
12.5	3.503	397.201
10	3.534	300.606

References

[1] Olivier C. Maes, Hyman M. Schipper, Howard M. Chertkow, Eugenia Wang. "Methodology for Discovery of Alzheimer's Disease Blood-Based Biomarkers". *Journal of Gerontology: Biological Sciences* 64A.6 (2009): 636-645. Available at http://biomedgerontology.oxfordjournals.org.ezproxy.wpi.edu/content/64A/6/636.

[2] Leonid Molochnikov, Jose M. Rabey, Evgenya Dobronevsky, et al. "A molecular signature in blood identifies early Parkinson's disease". *Molecular Degeneration* (2012). Available at http://www.molecularneurodegeneration.com.ezproxy.wpi.edu/content/7/1/26.

[3] F. Borovecki, L. Lovrecic, H. Jeong, F. Then, et al. "Genome-wide expression profiling of human blood reveals biomarkers for Huntington's disease". *Proceedings of the National Academy of Science* 102.31 (2005): 11023-11028. Available at http://www-ncbi-nlm-nih-gov.ezproxy.wpi.edu/pmc/articles/PMC1182457/.

[4] "Pathology Services Handbook, version 3.2.1". *St. George's Healthcare NHS Trust* (2013): 31-37. Available at http://www.stgeorges.nhs.uk/docs/pathology/handbook.pdf.

[5] H. Kobayashi, H. Ooi, Y. Yamada, M. Sakata, et al. "Serum CA125 level before the development of ovarian cancer". *International Journal of Gynecology and Obstetrics* 99 (2007): 95-99. Available at http://www.sciencedirect.com.ezproxy.wpi.edu/science/article/pii/S0020729207003189.

[6] Xinyan Bi, Shisheng Huang, Deny Hartono, Kun-Lin Yang. "Liquid-crystal based optical sensors for simultaneous detection of multiple glycine oligomers with micromolar concentrations". *Sensors and Actuators B* 127 (2007): 406-413. Print.

[7] Qiong-Zheng Hu, Chang-Hyun Jang. "A new strategy for imaging biomolecular events through interactions between liquid crystals and oil-in-water emulsions". *Analyst* 137 (2012): 5204-5207. Print.

[8] Alireza Hassanzadeh, Robert Lindquist. "Liquid Crystal Sensor Microchip". *IEEE Sensors Journal* 12 (2012): 1536-1544. Available at http://ieeexplore.ieee.org.ezproxy.wpi.edu/stamp/stamp.jsp?tp=&arnumber=6064864.

[9] Atul Dongre, Prajakta Bhisey, Khopkar Uday. "Polarized light microscopy". *Indian Journal of Dermatology, Venereology and Leprology* 73.3 (2007): 206-208. Available at http://www.bioline.org.br/abstract?id=dv07075.

[10] 19 July 2010. *Rays_passing_through_birefringent_material.svg*. Retrieved from https://en.wikipedia.org/wiki/File:Rays_passing_through_birefringent_material.svg.

[11] Graham Williams, Dale K. Thomas. "Phenomenological and Molecular Theories of Dielectric and Electrical Relaxation of Materials". *Novocontrol Application Note Dielectrics* 3 (1998). Print.

[12] Donald E. Barry. "Studies of Aggregation Pathways for Amyloidogenic Peptides by Dielectric Relaxation Spectroscopy". *Worceter Polytechnic Institute* (2013). Print.

[13] Helen Jansson, Rikard Bergman, Jan Swenson. "Role of Solvent for the Dynamics and the Glass Transition of Proteins". *The Journal of Physical Chemistry B* 115 (2011): 4099-4109. Print.

[14] Friedrich Kremer, Andreas Schönhals. *Broadband Dielectric Spectroscopy*. New York: Springer, 2003. Print.

[15] 29 April 2008. *Dielectric_responses.svg*. Retrieved from https://en.wikipedia.org/wiki/File:Dielectric_responses.svg.

[16] F. Kremer. "Dielectric spectroscopy - yesterday, today and tomorrow". *Journal of Non-Crystalline Solids* 305 (2002): 1-9. Print.

[17] Keven S. Paulson, et al. "Dielectric Relaxation Time Spectroscopy". *IEEE Transactions on Biomedical Engineering* 47.11 (2000): 1510-1517. Available at `http://ieeexplore.ieee.org.ezproxy.wpi.edu/xpls/abs_all.jsp?arnumber=880103&tag=1`.

[18] Jacques Rault. "Origin of the Vogel-Fulcher-Tammann law in glass-forming materials: the α-β bifurcation". *Journal of Non-Crystalline Solids* 271 (2000): 177-217. Print.

[19] M. Wolf, R. Gulich, P. Lunkenheimer, A. Loidl. "Relaxation dynamics of a protein solution investigated by dielectric spectroscopy". *Biochimica et Biophysica et Biophysica Acta - Proteins and Proteomics* (2012). Print.

[20] Kevin Lukas, Peter K. LeMaire. "Differential scanning calorimetry: Fundamental overview". *Resonance* 14.8 (2009): 807-817. Print.

[21] H. C. Watson. "The stereochemistry of protein myoglobin". *RCSB Protein Data Bank*. Rutgers, UCSD: 13 July 2011. `http://www.rcsb.org/pdb/explore/explore.do?structureId=1MBN`.

[22] "Differential Scanning Calorimetry (DSC)". *TA Instruments*. `http://thermophysical.tainstruments.com/`.

[23] J. Herrero-Albillos, F. Casanova, F. Bartolome. "Differential scanning calorimetry experiments in RCo_2". *Journal of Magnetism and Magnetic Materials* 290 (2005): 682-685. Print.

[24] G. Caliskan, A. Kisliuk, A. M. Tsai, C. L. Soles, A. P. Sokolov. "Influence of solvent on dynamics and stability of a protein". *Journal of Non-Crystalline Solids* 307-310 (2002): 887-893. Print.

[25] Wei Gu et al. "Molecular Dynamics Simulation of Hydration in Myoglobin". *Information Bridge: DOE Scientific and Technical Information* 103 (1995). Available at http://www.osti.gov/bridge/purl.cover.jsp?purl=/104441-RYIMcb/webviewable/.

[26] Jonathan B. Wittenberg, Beatrice A. Wittenberg. "Myoglobin function reassessed". *The Journal of Experimental Biology* 206 (2003): 2011-2020. Available at http://jeb.biologists.org/content/206/12/2011.

[27] Daniel J. Garry, George A. Ordway, John N. Lorenz, Nina B. Radford, Eva R. Chin, et al. "Mice without myoglobin". *Nature* 395 (2003): 905-908. Available at http://www.nature.com.ezproxy.wpi.edu/nature/journal/v395/n6705/full/395905a0.html.

[28] Randolph P. Cole. "Myoglobin Function in Exercising Skeletal Muscle". *Science* 216 (1982): 523-525. Available at http://www.jstor.org.ezproxy.wpi.edu/stable/1688296.

[29] 19 July 2012. *Myoglobin.png*. Retrieved from https://en.wikipedia.org/wiki/File:Myoglobin.png.

[30] G. W. Gray. "Liquid Crystals: Overview". *Encyclopedia of Materials: Science and Technology* (2001): 4570-4579. Print.

[31] 30 May 2008. *Nematic-Director.png*. Retrieved from https://en.wikipedia.org/wiki/File:Nematic-Director.png.

[32] Carl V. Brown. "Physical Properties of Nematic Liquid Crystals". *Handbook of Visual Display Technology* (2012): 1343-1361. Print.

[33] T. Bezrodna, V. Melnyk, V. Vorobjev, G. Puchkovska. "Low-temperature photoluminescence of 5CB liquid crystal". *Journal of Luminescence* 130 (2010): 1134-1141. Print.

[34] 2 October 2009. *4-Cyano-4'-pentylbiphenyl.svg*. Retrieved from https://en.wikipedia.org/wiki/File:4-Cyano-4'-pentylbiphenyl.svg.

[35] Steven Ellis, Germano Iannachionne. "The Phase Transitions of 4'-n-pentyl-4-cyanobiphenyl + C_{60} Colloidal Composites". *Worcester Polytechnic Institute* (2010). Available at `http://www.wpi.edu/Pubs/E-project/Available/E-project-042610-224416/`.

[36] Thimmaiah Govindaraju, Paul Bertics, et al. "Using Measurements of Anchoring Energies of Lipid Crystals on Surfaces to Quantify Proteins Captured by Immobilized Ligands". *Journal of the American Chemical Society* 129 (2007): 11223-11231. Print.

[37] Sharmistha Paul, Deepen Paul, et al. "Studies of Adsorption and Viscoelastic Properties of Proteins ono Liquid Crystal Phthalocyanine Surface Using Quartz Crystal Microbalance with Dissapation Technique". *Journal of Physical Chemistry C* 112 (2008): 11822-11830. Print.

[38] A. Hussain, A. S. Pina, A. C. A. Roque. "Bio-recognition and detection using liquid crystals". *Biosensors and Bioelectronics* 25 (2009): 1-8. Print.